J Sol-Gel Sci Technol (2009) 52:8–14
DOI 10.1007/s10971-009-2011-5

REVIEW

Structure and electrorheological properties of nanoporous $BaTiO_3$ crystalline powders prepared by sol–gel method

Wanquan Jiang · Chuanxia Jiang · Xinglong Gong · Zhong Zhang

Received: 10 April 2009 / Accepted: 1 June 2009 / Published online: 14 June 2009

Abstract In this paper, a novel nanoporous barium titanate ($BaTiO_3$) crystalline powder was synthesized by using triblock poly(ethylene oxide) (PEO) and poly(propylene oxide) (PPO) based systems (P-123) as the soft template via a sol–gel method and their structure-dependent electro rheological property was studied. The pore diameter and specific surface area of $BaTiO_3$ were precisely controlled by varing the calcined temperature. The chemical composition, structure and surface morphology of $BaTiO_3$ were characterized by X-ray diffraction (XRD), thermo gravimetric analysis (TGA), and nitrogen adsorption–desorption method, scanning electron microscopy (SEM) and transmission electron microscopy (TEM). The result revealed that the pore volume and specific surface area of $BaTiO_3$ decreased with the increment of calcined temperature. The electro rheological fluids (ERFs) were obtained by dispersing $BaTiO_3$ crystallites in silicon oil and three kinds ERFs were fabricated by using three kinds of $BaTiO_3$ which were prepared under different calcined temperature (550, 600 and 900 °C) as the precursors. The behaviors of the ERFs were evaluated via a rotational rheometer fixed with electric field generator. The results showed that electro rheological effect was related to the pore volume and specific surface area of $BaTiO_3$. Due to the distinct advantage of sol–gel method for preparing nanoporous $BaTiO_3$ without contamination of the materials, the markedly low current destiny of the ERFs was obtained. The yield stress of ERFs with large specific surface area of $BaTiO_3$ reached the maximum of 3 kPa, which is higher than that of ERFs using traditional pure $BaTiO_3$ crystallites (lower than 1 kPa).

Keywords Porous · $BaTiO_3$ · Electrorheological properties · Sol–gel

W. Jiang (✉) · C. Jiang
Department of Chemistry, University of Science and Technology of China (USTC), Hefei 230026, People's Republic of China
e-mail: jiangwq@ustc.edu.cn

X. Gong (✉)
CAS Key Laboratory of Mechanical Behavior and Design of Materials, Department of Modern Mechanics, University of Science and Technology of China (USTC), Hefei 230027, People's Republic of China
e-mail: gongxl@ustc.edu.cn

Z. Zhang
National Center for Nanoscience and Technology, Beijing 100080, People's Republic of China

1 Introduction

Barium titanate ($BaTiO_3$) with excellent dielectric, ferroelectric and piezoelectric properties have been widely used in modern electronic devices, such as transducers, dense ferroelectrics, thin-film electronic components and multilayer ceramic capacitor [1–3]. Over the past decade, lots of works have been reported about the synthesis of $BaTiO_3$ crystalline with different morphologies as: nanotubes, nanorods, nanowires and nanofibers [4–7]. Mesoporous and porous materials have important characteristics that they have possession of large surface areas and nanosize porous structure [8]. These characteristics make these materials widely used in photoelectronics, catalystic reactions, semiconductors, and so on [9, 10]. Thus, much attention has been focused on the preparation of mesoporous $BaTiO_3$ and studied on their structure-dependent property.

Up to now, various methods have been developed for the preparation of mesoporous and porous materials, including solid–liquid method [11], microwave-assisted esterification route [12], ultrasound-assisted method [13], microwave-hydrothermal route [14], polymeric precursor method [15], hydrothermal method [16], hydrothermal-electrochemical method [17], a soft-template approach [18], and sol-precipitation method. However, the reported preparation routes of porous $BaTiO_3$ were very seldom. For example, mesoporous $BaTiO_3$ was prepared by Hou's group using sol-precipitation method [19]. This synthetic way was very complicated and time-consuming which limited practical application. Therefore, more methods should be developed to synthesis $BaTiO_3$ crystalline powder with mesoporous nanostructure.

Sol–gel approach, as a classical method, has a lot of inherent merits with better homogeneity, higher purity, and lower temperature of preparation. A number of materials, such as silica, alumina, carbons, TiO_2 and other metal oxides [20–23] with mesoporous nanostructure have been successfully fabricated by using this method. In this work, considering its various advantages, sol–gel method was employed to synthesize mesoporous $BaTiO_3$ crystalline powder by using P-123 as a block copolymer template, for its attractive advantage of lower cost, lower toxicity, and ease of template removal [24]. To the best of our knowledge, this is the first report about the preparation of mesoporous $BaTiO_3$ by using P-123 as a template.

Additionally, $BaTiO_3$ has a high dielectric property, which is suitable for fabrication of electrorheological fluids (ERFs). ERFs are composed of dielectric particles from nano-sized to micro-sized suspended in insulating medium. The typical feature of ERFs is that apparent viscosity can be experienced a rapid, reversible change by applying an external electric field. That can be defined by using the formula as follows: $\eta_B = \eta_0 + \Delta\eta = \eta_0 + \tau_E/\gamma$ (η_B is the apparent viscosity with applying an external electric field, η_0 is the apparent viscosity in the absence of electric field strength, $\Delta\eta$ is the viscosity which caused by applying external electric field, τ_E is the shear stress, γ is shear rate), As a result of the ability to control the apparent viscosity electrically, ERFs are considered to have many potential applications in the field of industry, such as: clutches, dampers, valves, seismic resistance and so on [25–27]. Consequently, more work should be done on the synthesis of $BaTiO_3$ material with high dielectric property for they are considered as a potential candidate of the new high-performance ER material. In this study, besides obtaining a novel type of nanoporous $BaTiO_3$ material, we also investigated the properties of ERFs based on nanoporous $BaTiO_3$ crystallites with different morphology structure.

2 Experimental

2.1 Materials

Tetrabutyl titanate (TBT, >98%), acetic acid (CH_3COOH), barium acetate ($Ba(Ac)_2$), silicone oil were purchased from Sinopharm Chemical Reagent Company (Shanghai, China). Poly(ethylene glycol)-block-poly(propylene glycol)-block-poly(ethylene glycol) (P-123) was obtained from Sigma-Aldrich incorporation (St. Louis, USA). All chemicals were of analytical grade and used without further purification. Doubly deionized water was used through all the processes.

2.2 Synthesis of nanoporous $BaTiO_3$

Mesoporous $BaTiO_3$ particles were synthesized by sol–gel process using P-123 as a template. In a typical synthesis, $Ti(OBu)_4$ (0.05 mol) was firstly dissolved in glacial acetic acid (10 mL) at room temperature 25 °C as solution 1. Then, $Ba(Ac)_2$ (0.05 mol), ethyl alcohol (10 mL) and H_2O (2 mL) were dissolved in glacial acetic acid (30 mL) as solution 2. These two solutions were mixed together to prepare the precursor of $BaTiO_3$ under magnetic stirring for 1 h, the temperature was increased to 80 °C while a gel-like product was obtained. Finally, $BaTiO_3$ powders were successfully achieved by treating the gel-like product under 550, 600, and 900 °C for 2 h, respectively.

2.3 Preparation of nanoporous $BaTiO_3$ ER suspensions

Prior to the preparation of ER suspensions, the silicone oil (dielectric constant (ε_f) = 2.60–2.80, density = 0.975 g/cm^3, viscosity = 500cPs, temperature = 25 °C) was first dried at 100 °C to remove the H_2O 2 h, then as-prepared $BaTiO_3$ at different calcined temperature (550, 600 and 900 °C) were dispersed in silicone oil by ball milling, respectively. The milling process was sustained for 24 h. Finally, three kinds of white ER suspensions under different calcined temperature's $BaTiO_3$ particles (550, 600 and 900 °C), with the same volume fraction of 30% were collected for further characterization.

2.4 Characterization

Thermal behavior of the gel ($BaTiO_3$) was examined by thermogravimetric analysis (DTG-60H, Japan) under air atmosphere. The heating rate and flow rate is 5 °C/min and 50 mL/min, respectively. The nitrogen (N_2) adsorption/desorption isotherms at about 77 k were studied dispending Micromeritics, ASAP 2020 M system. In the first step, the

particles must be degassed at 350 °C under vacuum for 5 h, and then, the specific surface area was calculated by Brunauer-Emmett-Teller (BET) method and the range of a P/P^0 is changed from 0.06 to 0.20. X-ray diffraction (XRD) patterns were obtained by a Rigaku diffactometer (MXPAHF, Japan) with Cu$K_\alpha$radiation ($\lambda = 0.15406$ nm). The scanning rate of the diffactometer is 8°/min. The measurement was carried out by a generator with a voltage of 40 kV and a current of 100 mA. The morphology of the powders was observed with a scanning electron microscopy (SEM, Sirion 200, Holland) operating at 5 kV. The microstructure of the particles was investigated by a transmission electron microscopy (TEM, JEM-2100F, Japan). A rotational rheometer (Physica, MCR 301, Anton Paar, Austria, the gap between the outer barrel and the inner probe was 0.42 mm) with the ER HVS/ERD180 and CC10-E accessory were used to measure the rheological characteristics of the ERF, where the ERF was placed into the barrel in between the two concentric circles. The rotational rheometer equipped with a temperature control accessory Physica VT2 was used to measure the temperature dependence of shear stress.

3 Results and discussion

3.1 Synthesis and characterization of nanoporous $BaTiO_3$

In our system, porous $BaTiO_3$ material was synthesized by using an improved sol–gel approach. Figure 1 shows the TGA-DTA curve of the $BaTiO_3$ wet gel and Fig. 2 shows the XRD patterns of the $BaTiO_3$ crystalline powder synthesized at diffrent calcinations temperature respectively. As is shown in Fig. 1, within the range of 40–160 °C, the weight loss was approximately 41.73% in the TGA curve, in the meanwhile, two endothermic peaks at 79 °C and 139 °C in the DTA curve can also be found because of the dehydration and evaporation of ethanol, acetic acid and water [28]. The weight loss at 160–320 °C was about 21.62% in the TGA curve related to an exothermic peak at 272 °C in the DTA curve. It can be explained by the oxidizing combustion of butoxy in the gel [3, 29], with the range of 320–450 °C, the weight loss was about 8.83% in the TGA curve, as well as an exothermic peak at 368 °C in the DTA curve is attributed to the decomposition of P-123 block [30]. The XRD results were well agreed with the above analysis. The XRD curves in Fig. 2 show that the TiO_2 and $BaCO_3$ phases are appeared and the broad peak of P-123 block is disappeared at 450 °C. In the TGA curve, the weight loss at 450–650 °C is about 2.09%, owing to the formation of $BaTiO_3$ and the release of CO_2 by the reaction between $BaCO_3$ and TiO_2 [31]. Corresponding to the XRD

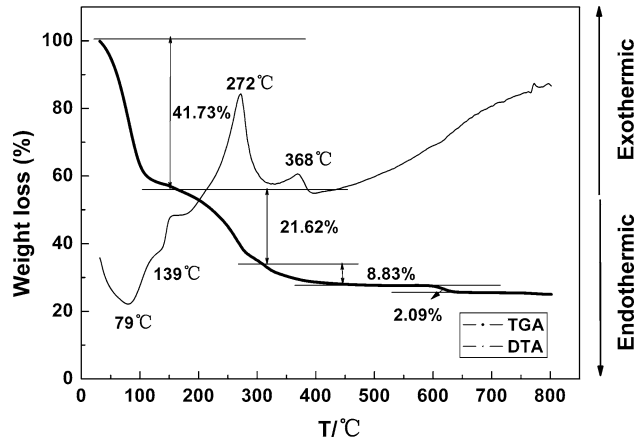

Fig. 1 TGA and DTA curves of $BaTiO_3$ gel

curves at 550 and 600 °C, the presence of diffraction peaks can be used to evaluate the structural order at long rang [32]. $BaTiO_3$ phase was confirmed by comparing XRD patterns with the respective Joint Committee on Powder Diffraction Standards (JCPDS) card No. 05–0626. All the diffraction peaks are related with tetragonal structure, although, a small $BaCO_3$ phase can also be found. After 650 °C, no weight loss is found in Fig. 1 related to XRD patterns at 900 °C, which indicated that the well-crystallized and pure $BaTiO_3$ phase is formed.

Figure 3 shows the nitrogen adsorption/desorption isotherms and BJH pore size distributions (inset) of nanoporous $BaTiO_3$ samples calcined at 550, 600 and 900 °C, respectively. All three curves show a single and narrow hysteresis loop. These may be because of the special one-end open shape of the pore structure creating the similar initial pressure of evaporation and capillary condensation. The similar experimental results were found in reference

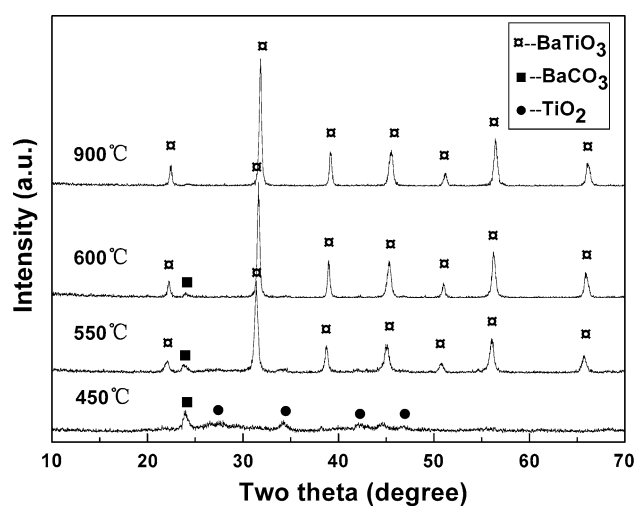

Fig. 2 XRD patterns of $BaTiO_3$ gel at different calcined temperatures

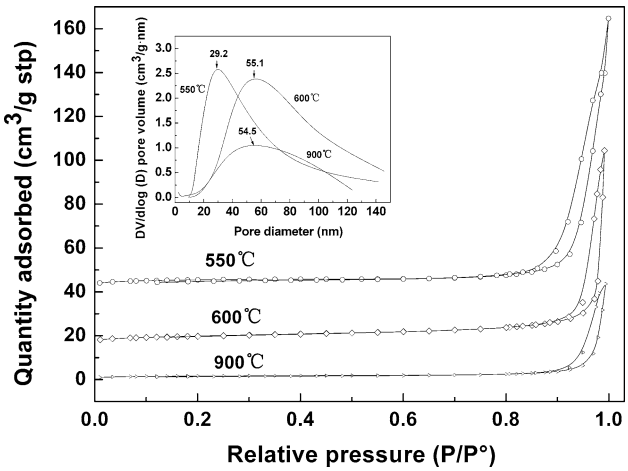

Fig. 3 The nitrogen adsorption/desorption isotherms and BJH pore size distributions (inset) of nanoporous $BaTiO_3$ samples under different calcined temperature

Table 1 Porosity and grain size of $BaTiO_3$ prepared under different calcined temperature

T (°C)	S_{BET} (m^2/g)	V_t (cm^3/g)	Pore size (nm)	Grain size (nm)
550	18.8	0.10	29.2	83
600	17.1	0.04	>50	134
900	5.60	0.02	>50	200

[19]. The BET specific surface areas and total pore volumes are calculated using Brunauer-Emmett-Teller (BET) equation, however, the pore diameters which were calculate using Barrett-Joyner-Halenda (BJH) method from desorption branches of isotherms. Furthermore, the BET specific surface areas (S_{BET}), total pore volumes (V_t), and the pore diameters of the porous $BaTiO_3$ at different calcined temperature are summarized in Table 1. We can conclude from table 1 that with the rising of the temperature, the BET specific surface areas are declined from 18.8 to 5.6 m^2/g and the total pore volumes are reduced from 0.10 to 0.02 cm^3/g. When the calcined temperature is 550 °C, the pore size is pecked at 29.2 nm which is less than 50 nm corresponding to the inset in Fig. 3. Thus, we can conclude that the $BaTiO_3$ sample calcined at 550 °C is a mesoporous material and the mesoporous structures can be observed (arrows point to) from Fig. 5a. However, when the calcined temperature are at 600 and 900 °C, the pore diameters are both higher than 50 nm (inset in Fig. 3) and the porous structures can not be noticed apparently from Fig. 5b, c. This may be due to the aggregation of the particles resulting from the forming of compact aperture.

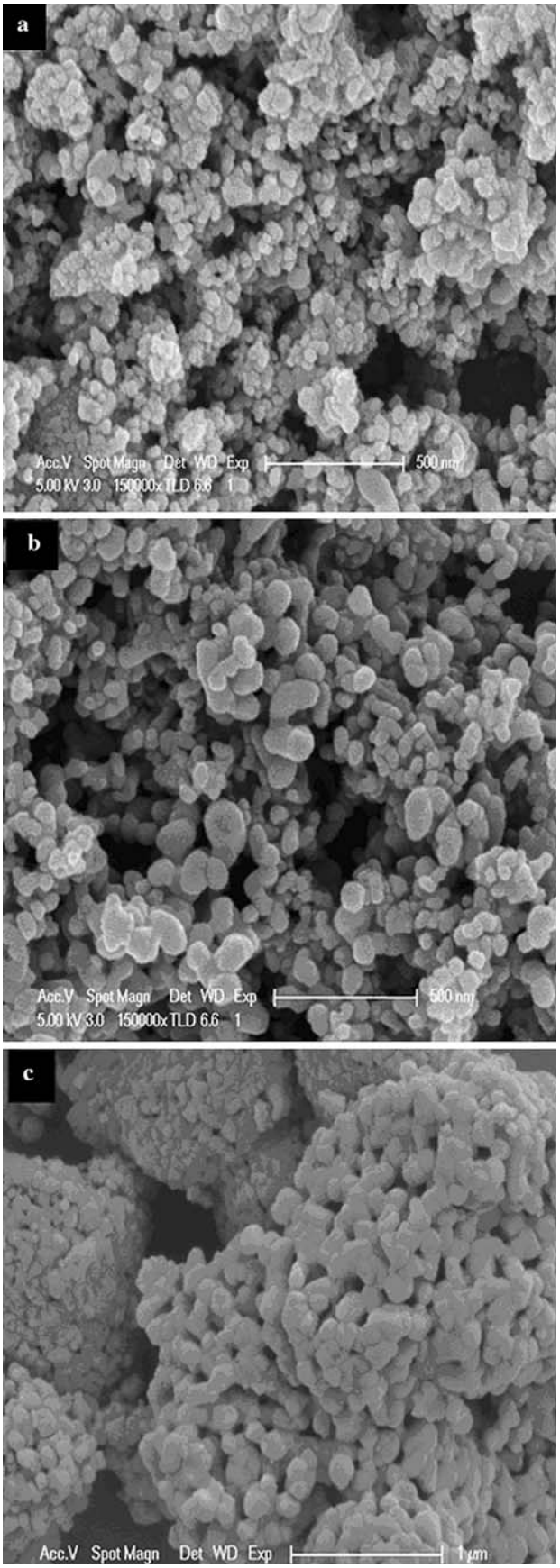

Fig. 4 The surface morphology of nanoporous $BaTiO_3$ under different calcined temperature (**a** 550 °C, **b** 600 °C, **c** 900 °C) viewed by SEM, respectively

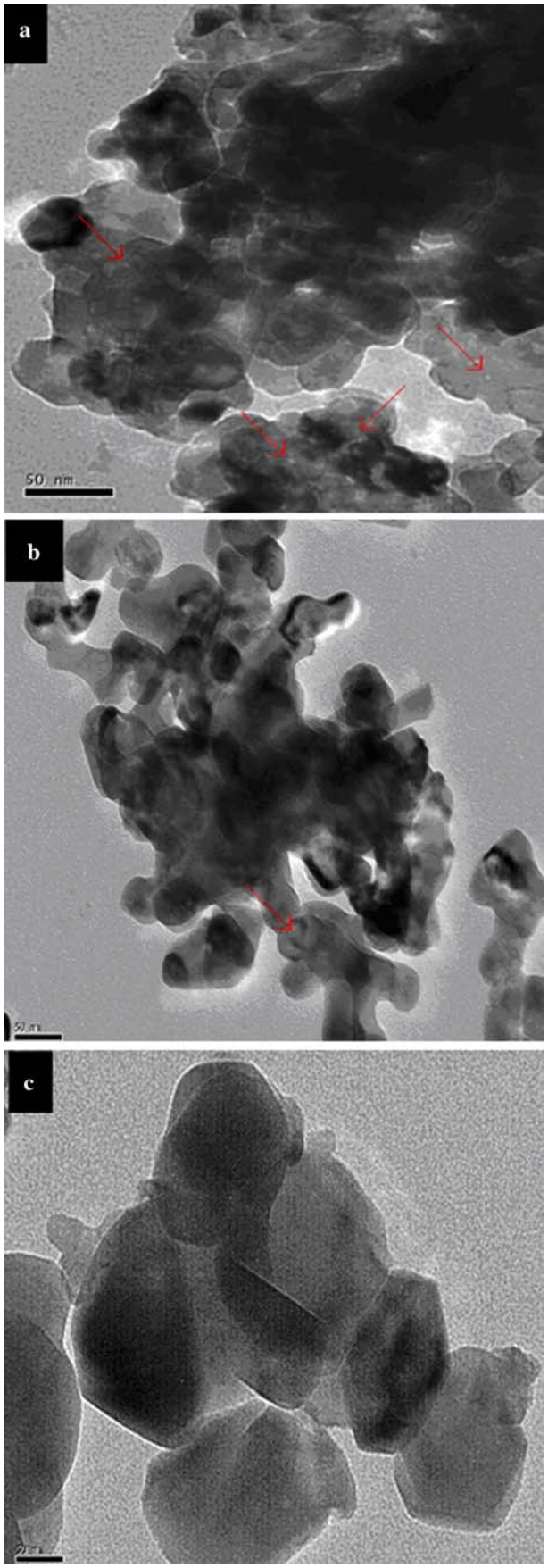

◀**Fig. 5** The microstructure of nanoporous $BaTiO_3$ under different calcined temperature (**a** 550 °C, **b** 600 °C, **c** 900 °C) viewed by TEM, respectively

The morphologies and microstructures of nanoporous $BaTiO_3$ particles were further characterized by SEM and TEM images, respectively (Figs. 4, 5). From Fig. 4a–c, we can find that all the particles present an agglomerate nature. Furthermore, the particles growth was suppressed with the temperature decreased. The reason probably can be explained that the agglomerate nature of the particles can be related to the residual organic compounds during the pyrolysis process [33]. Figure 5 shows the high resolution TEM image of the $BaTiO_3$ particles which were synthesized by different temperature and the grain sizes of as-prepared $BaTiO_3$ were also summarized in Table 1. It can be seen from Fig. 5a–c that the grain sizes are increased from 83 to 200 nm with the calcined temperature increases, which are consistent with the SEM analysis.

3.2 Electrorheolegical properties of as-prepared nanoporous $BaTiO_3$

The Electrorheolegical properties of as-prepared porous $BaTiO_3$ samples were also investigated in this study. The flow curves of the yield stress versus electric field strength for 30 vol% ER fluids containing different particles (calcined at 550, 600, and 900 °C, respectively.) are shown in Fig. 6. The related current densities are shown in the small inset. We can manifest from the results that with the calcined temperature of particles increases, the electrorheological effect is increased. Thus, the ER fluid exhibited the highest ER effect at 550 °C, while the lowest ER effect

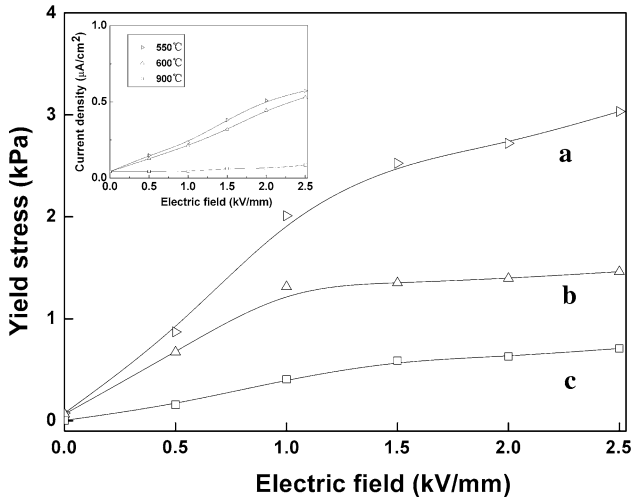

Fig. 6 The yield stress measured as a function of electric field strength for 30 vol% ER fluids containing different particles: nanoporous $BaTiO_3$ 550 °C (a), 600 °C (b), 900 °C (c). The current densities related to those samples are shown in the small inset

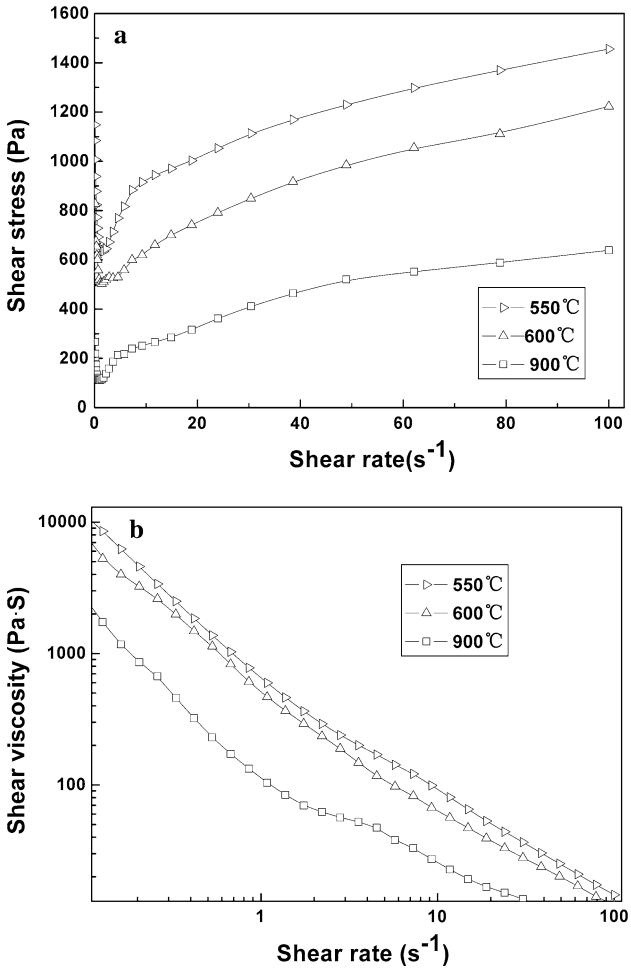

Fig. 7 Flow curves of the shear stress **a** and viscosity **b** versus shear rate for 30 vol% ER fluids containing different particles (calcined at 550, 600, and 900 °C, respectively.) at the same electric fields with 2 kV/mm

at 900 °C. At the electric field of E = 2.5 kV/mm, the yield stress was up to about 3 kPa. The effect of the temperature on the ER effect may be due to the particles with the larger surface area at low calcined temperature. The oleophilic of particles with silicone oil is improved. It can be concluded that larger surface area induces larger wettability resulting in higher ER activity [34]. The inset also indicates that the related current densities are very low, which implies that low current densities are very critical for electrorheological fluid [29]. The lower the current densities, the better the ER activity.

Figure 7 shows the flow curves of the shear stress (a) and viscosity (b) versus shear rate for 30vol% ER fluids containing different particles (calcined at 550, 600, and 900 °C, respectively.) at the same electric fields with 2 kV/mm. As is shown in Fig. 7a, the shear stress decreases distinctly in the low shear rate region. The shear stress of the suspension increases with the shear rate in the high shear rate region

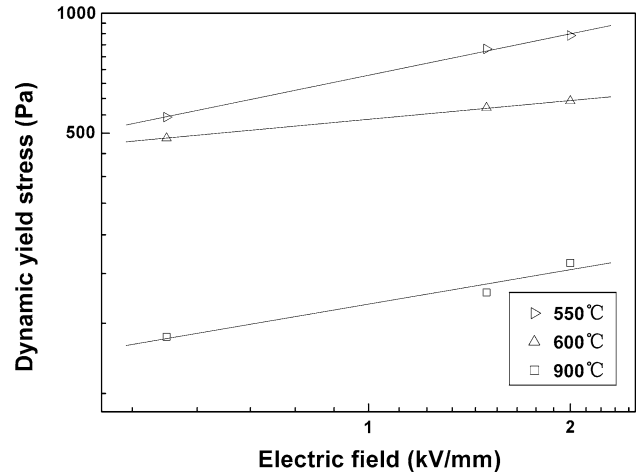

Fig. 8 The dynamic yield stress versus electric field strength for 30 vol% ER fluids containing particles calcined at different temperature

(>1 s^{-1}). It can be seen in Fig. 7b that the shear viscosity of the ER fluids containing particles calcined at 550 °C is higher than that of other ER fluids in the entire shear rate range. Furthermore, when the shear rate is above 1/s, i.e., $\dot{\gamma} > 1\ s^{-1}$, ER fluids exhibit shear thinning behavior, similar to common ER suspensions [34, 35].

For further characterizing ER effect, a Bingham model was used to find the electric field-dependence of dynamic yield stress. Figure 8 is the variation of the dynamic yield stress (τ_y) with the external electric field (E). Three plots reveal that the relationship between dynamic yield stress and the electric field strength can be described as $\tau_y \propto E^{\alpha}$. The α values of the ER fluids containing particles calcined at 550, 600, and 900 °C are 0.35, 0.16, 0.29, respectively, which is different from electrostatic polarization model [36]. This may be due to the irregular particle shape and the broad particle size distribution, which can be observed through SEM, TEM, in Figs. 4 and 5.

4 Conclusion

In this study, a novel nanoporous $BaTiO_3$ with crystalline structure was obtained by sol–gel method. Nitrogen adsorption–desorption method, SEM and TEM indicated that the particles possess a porous structure with a specific surface area. And the TGA-DTA curve demonstrated the formation temperature of the particles. Furthermore, the electrorheological activities of these were studied and the influence of special surface area on the electrorheological effect was also discussed. The results of the study showed that the ER suspension exhibited better ER properties with low current density and the electrorheological effect were improved with the special surface area increasing. The ER

effect of the ERFs with nanoporous $BaTiO_3$ calcined at 550 °C was several times higher than that of ERFs with particles calcined at 900 °C. The increasing of the ER effect was attributed to the better wettability and thus the study can help for designing new high-performance ER materials.

Acknowledgments Financial support from National Basic Research Program of China (973 Program, Grant No. 2007CB936800) is gratefully acknowledged.

References

1. Satoshi O, Akira K, Hirofumi S, Kazuyoshi S, Hiroya A, Makio N (2008) Mater Lett 62:2957. doi:10.1016/j.matlet.2008.01.083
2. Fang CY, Wang CP, Polotai AV, Agrawal DK, Lanagan MT (2008) Mater Lett 62:2551. doi:10.1016/j.matlet.2007.12.045
3. Cui B, Yu PF, Wang X (2008) J Alloy Comp 459:589. doi:10.1016/j.jallcom.2007.07.039
4. Chen YY, Yu BY, Wang JH, Cochran RE, Shyue JJ (2009) Inorg Chem 48:681. doi:10.1021/ic8018887
5. Zhang SY, Jiang FS, Qu G, Lin CY (2008) Mater Lett 62:2225. doi:10.1016/j.matlet.2007.11.055
6. Wang ZY, Hu J, Yu MF (2006) Appl Phys Lett 89:263119. doi:10.1063/1.2425047
7. Yuh JH, Nino JC, Sigmund WM (2005) Mater Lett 59:3645. doi:10.1016/j.matlet.2005.07.008
8. Larsen G, Lotero E, Nabity M, Petkovic LM, Shobe DS (1996) J Catal 164:246. doi:10.1006/jcat.1996.0379
9. Victor F, Stone J, Davis RJ (1998) Chem Mater 10:1468. doi:10.1021/cm980050r
10. Corma A (1997) Chem Rev 97:2373. doi:10.1021/cr960406n
11. Zheng MB, Cao J, Liao ST, Liu JS, Chen HQ, Zhao Y, Dai WJ, Ji GB, Cao JM, Tao J (2009) J Phys Chem C 113:3887. doi:10.1021/jp810230d
12. Li YF, Li HF, Li TH, Li GL, Cao R (2009) Microporous Mesoporous Mater 117:444. doi:10.1016/j.micromeso.2008.06.042
13. Li H, Ni YH, Cai YF, Zhang L, Zhou JZ, Hong JM, Wei XW (2009) J Mater Chem 19:594. doi:10.1039/b818574c
14. Moreira ML, Mambrini GP, Volanti DP, Leite ER, Orlandi MO, Pizani PS, Mastelaro VR, Paiva-Santos CO, Longo E, Varela JA (2008) Chem Mater 20:5381. doi:10.1021/cm801638d
15. Orhan E, Varela JA (2005) Phys Rev B 71:085113. doi:10.1103/PhysRevB.71.085113
16. Wang YG, Xu G, Yang LL, Ren ZH, Wei X, Weng WJ, Du PY, Shen G, Han GR (2009) Mater Lett 63:239. doi:10.1016/j.matlet.2008.09.050
17. Wu ZB, Yoshimura M (1999) Solid State Ion 122:161. doi:10.1016/S0167-2738(99)00030-2
18. Yamauchi Y, Kuroda K (2008) Chem Asian J 3:664. doi:10.1002/asia.200700350
19. Hou RZ, Ferreira P, Vilarinho PM (2008) Microporous Mesoporous Mater 110:392. doi:10.1016/j.micromeso.2007.06.051
20. Zhang J, Ma YB, Shi F, Liu LQ, Deng YQ (2009) Microporous Mesoporous Mater 119:97. doi:10.1016/j.micromeso.2008.10.003
21. Sun ZX, Zheng TT, Bo QB, Vaughan D, Warren M (2008) J Mater Chem 18:5941. doi:10.1039/b810202c
22. Lia LX, Zou LD, Song HH, Morris G (2009) Carbon 47:775. doi:10.1016/j.carbon.2008.11.012
23. Tsai MC, Chang JC, Sheu HS, Chiu HT, Lee CY (2009) Chem Mater 21:499. doi:10.1021/cm802327z
24. Lee B, Yamashita T, Lu DL, Kondo JN, Domen K (2002) Chem Mater 14:867. doi:10.1021/cm010775m
25. Block H, Kelly JP (1988) J Phys D Appl Phys 21:1661. doi:10.1088/0022-3727/21/12/001
26. Wei JH, Zhao LH, Peng SL, Shi J, Liu ZY, Wen WJ (2008) J Sol–Gel Sci Technol 47:311. doi:10.1007/s10971-008-1787-z
27. Gong XQ, Wu JB, Huang XX, Wen WJ, Sheng P (2008) Nanotechnology 19:165
28. Lopes KP, Cavalcante LS, Simões AZ, Varela JA, Longo E, Leite ER (2009) J Alloy Comp 468:327. doi:10.1016/j.jallcom.2007.12.085
29. Yu PF, Cui B, Shi QZ (2008) Mater Sci Eng A 473:34. doi:10.1016/j.msea.2007.03.051
30. Yin JB, Zhao XP (2002) Chem Mater 14:4633. doi:10.1021/cm020388s
31. Cui B, Yu PF, Wang X (2008) J Alloy Comp 459:589. doi:10.1016/j.jallcom.2007.07.039
32. Marques VS, Cavalcante LS, Sczancoski JC, Volanti DP, Espinosa JWM, Joya MR, Santos MRMC, Pizani PS, Varela JA, Longo E (2008) Solid State Sci 10:1056. doi:10.1016/j.solidstatesciences.2007.11.004
33. Nunes MGB, Cavalcante LS, Santos V, Sczancoski JC, Santos MRMC, Santos-Júnior LS, Longo E (2008) J Sol–Gel Sci Technol 47:38. doi:10.1007/s10971-008-1751-y
34. Wang BX, Zhao Y, Zhao XP (2007) Colloids Surf A Physicochem Eng Asp 295:27. doi:10.1016/j.colsurfa.2006.08.025
35. Kim SG, Kim JW, Jang WH, Choi HJ, Jhon MS (2001) Polymer (Guildf) 42:5005. doi:10.1016/S0032-3861(00)00887-9
36. Klingenberg DJ, Vanswol F, Zuoski CF (1991) J Chem Phys 94:6170. doi:10.1063/1.460403